Initial Characterization of the 30 kW Miniature Arc Jet (mARC II) at NASA Ames Research Center

Megan E. MacDonald[1]
Jacobs Technology at NASA Ames Research Center, Moffett Field, California, 94035

Magnus A. Haw[2]
AMA Inc. at NASA Ames Research Center, Moffett Field, California, 94035

Daniel Philippidis[3]
NASA Ames Research Center, Moffett Field, California, 94035

Daniel E. Schickele[4]
Jacobs Technology at NASA Ames Research Center, Moffett Field, California, 94035

Diana Z. F. Luis[5]
NASA International Internship Program at NASA Ames Research Center, Moffett Field, California, 94035

Joe Hartman[6]
Sierra Lobo Inc. at NASA Ames Research Center, Moffett Field, California, 94035

Mark S. McGlaughlin[7]
NASA Ames Research Center, Moffett Field, California, 94035

The second-generation Miniature Arc jet Research Chamber (mARC II) at NASA Ames is undergoing integrated systems testing. Once fully operational, this facility will be added to the range of available test facilities operated by the NASA Ames Thermophysics Facilities Branch, with primary focus on applications such as new arc jet flow diagnostics and new arc column diagnostics. Initial characterization of the mARC II is reported here, specifically, measured arc current, arc voltage, column and chamber pressures, mass flow rates, and initial emission measurements carried out at a range of conditions.

Nomenclature

ARC = Ames Research Center
mARC II = miniature Arc jet Research Chamber (second-generation)
NASA = National Aeronautics and Space Administration
TPS = thermal protection system

[1] Senior Aerospace Engineer, Thermophysics Facilities Branch, NASA Ames Research Center, MS 229-4, Member AIAA.
[2] Plasma Physicist, Thermal Protection Materials Branch, NASA Ames Research Center.
[3] Senior Engineer, Thermophysics Facilities Branch, NASA Ames Research Center, MS 229-4.
[4] Engineer, Thermophysics Facilities Branch, NASA Ames Research Center, MS 229-4.
[5] Research Intern, Thermophysics Facilities Branch, NASA Ames Research Center.
[6] Senior Engineering Consultant, Thermophysics Facilities Branch, NASA Ames Research Center, MS 229-4.
[7] EAST and mARC Facilities Manager, Thermophysics Facilities Branch, NASA Ames Research Center, MS 229-4.

I. Introduction

Arc jets are ground test facilities that are frequently used to produce continuous flows of high-speed plasma for testing and certification of high-temperature materials. An arc jet uses a confined electric arc discharge to heat a flowing test gas to high enthalpy. This gas is then accelerated through a nozzle, into a low-pressure test chamber, and over a sample of material at supersonic speeds. Through direct exposure to these simulated high-altitude atmospheric entry conditions, material samples can be evaluated for their ability to survive atmospheric entry. The NASA Ames Thermophysics Facilities Branch operates six high-power (10 – 60 MW) arc heaters in four different arc jet test bays [1]. Operational complexity inherently accompanies these high-power facilities. Some test programs do not require large-scale facilities and are better suited to testing on a smaller scale. Various reasons could drive this, from limited budget (a smaller facility is less costly to operate) to the ability to test a large number of materials or instruments in a short time. The miniature Arc jet Research Chamber (mARC) facility was created to reproduce in a small scale ground test the aerodynamic heating experienced by a flight vehicle at high flight speeds and altitudes. This arc jet can serve as a test bed for exploring new diagnostics, sensors, and even materials at conditions relevant to the high-power arc jets, but on a much smaller scale and at a lower operating cost, requiring fewer operations personnel and less facility maintenance.

The history of the mARC II facility has been described previously [2]. It was recently upgraded and is currently undergoing integrated systems testing. The purpose of this manuscript is to report initial data taken as the facility is brought online. Figure 1 shows the jet as it exits the nozzle and expands into the vacuum chamber at two different arc current settings. On the left are the flange and bolt heads that hold the arc heater to the chamber. In the background behind the jet is the window through which spectroscopic emission measurements are made. As will be discussed, the chamber pressure in the current configuration is higher than optimal, so Fig. 1 shows the jet slightly over-expanded. In optimal configuration, this jet will run under-expanded.

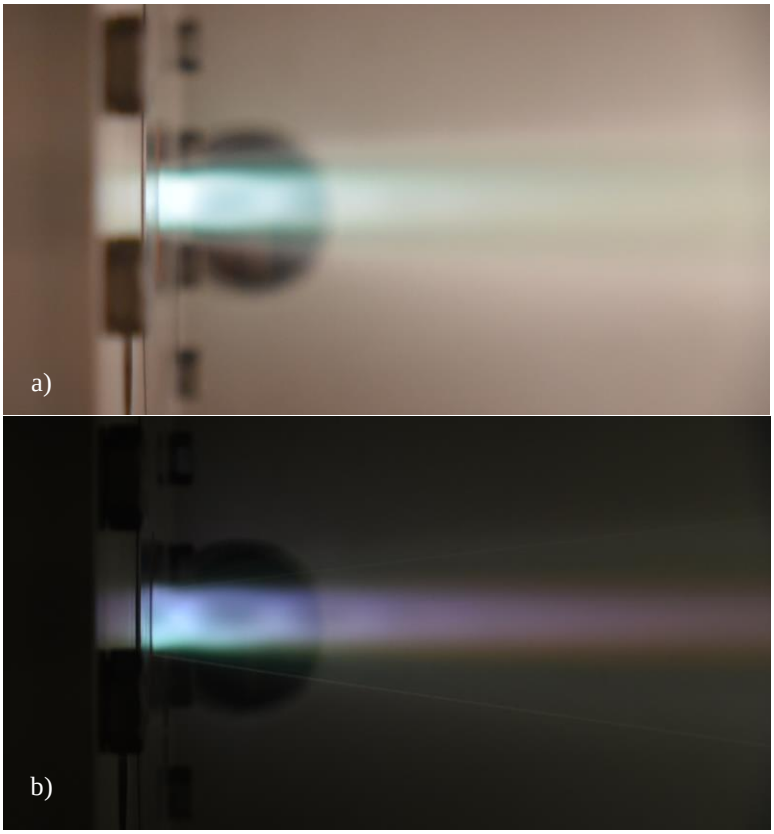

Figure 1: Photos of the mARC II jet. a) mARC001 Run 14: 40A, 0.25 g/s air (1/60 sec, f/2.8, 35 mm, ISO 1600, with UV filter); b) mARC001 Run 20: 100A, 0.25 g/s air (1/20 sec, f/6.3, 25 mm, ISO 200 with UV filter)

II. Experimental Setup

A. Arc Heater

The mARC II arc heater is a segmented constricted arc heater. It is composed of a Hypertherm MAX200 hand torch main body (into which the cathode is mounted), a strongback to hold all of the arc heater components together, one standard constrictor disk, one constrictor disk with a pressure tap, the anode, and a converging-diverging nozzle. The strongback, constrictor disks, anode, and nozzle have been fabricated from oxygen free high conductivity copper (ASME SB-187). Each component is insulated from the adjacent component by a boron nitride disk. The layout of the heater is shown in Fig. 2. In its current configuration, the heater is assembled with two constrictor disks as shown. Aside from the nozzle, the geometry of this heater matches that of the first-generation mARC [3], but the new mARC II design includes water cooling for each component. Further detail on active cooling of the arc column is given in Refs. 2 and 3.

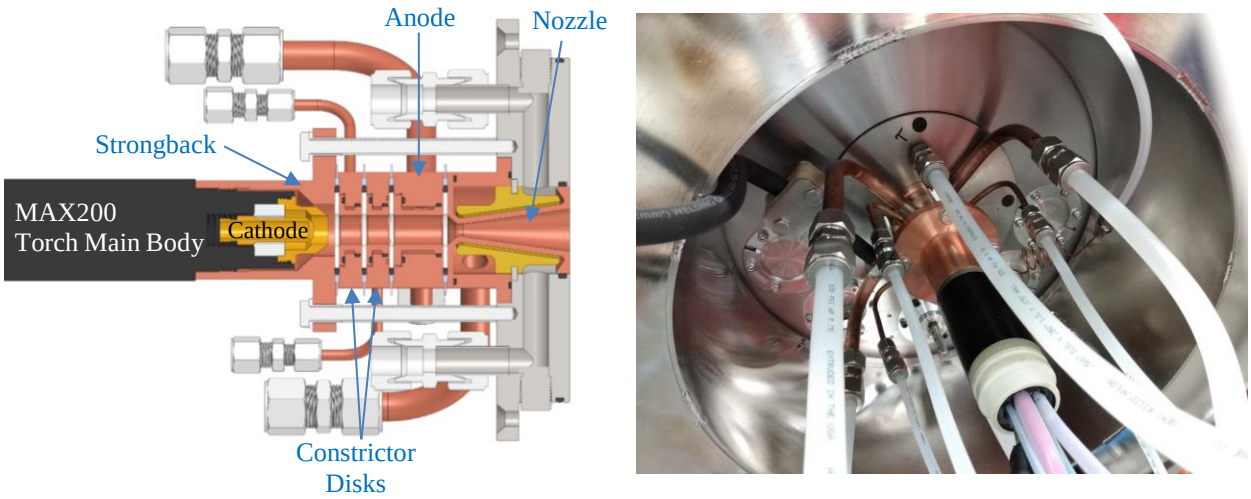

Figure 2: mARC II Arc Heater. Left image is a CAD cross section and right image is as-built.

B. Support Infrastructure

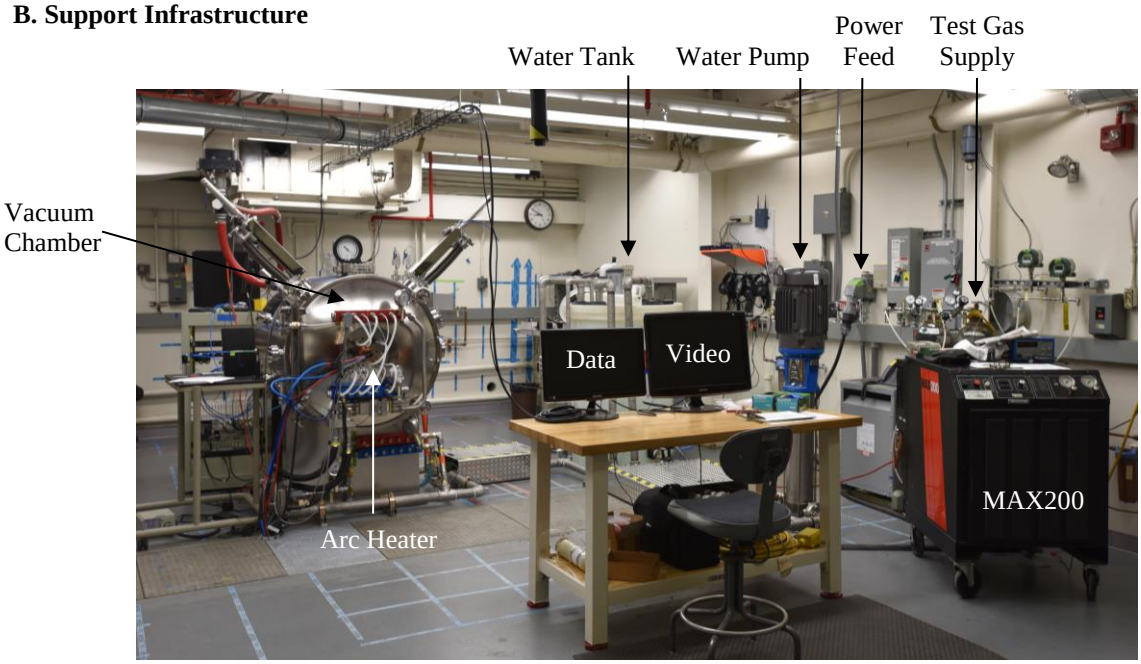

Figure 3: Overview of the mARC II system

The mARC II cooling system consists of four coolant loops. The first cools the arc heater and the vacuum chamber. 750 liters of distilled water is stored in a tank adjacent to the chamber and is recirculated through the heater and chamber walls with a Goulds Model e-SV pump at approximately 150 l/m. A temperature difference sensor and flowmeter are installed on this loop to provide an estimate of bulk enthalpy delivered to the plasma. This water tank and water pump are shown in Fig. 3 as indicated. The second cooling loop is contained within the MAX200 unit. This 30% propylene glycol, 70% deionized water mixture cools only the cathode at a flow rate of 3 l/m. The third cooling circuit uses tap water to cool the vacuum pump and the heat exchanger at a flow rate of approximately 11 l/m. In Fig. 3, it is on the far wall, but is blocked from view by the vacuum chamber. The fourth cooling circuit is a 45-liter high-pressure mobile recirculating cooling system that pumps distilled water at up to 5.7 l/m to cool the sensors during their insertion into the jet flow. This is not shown in Fig. 3.

Gas is supplied to the system through the MAX200 controller. Up to two different gases (K-cylinders) are plumbed through Sage Prime (SIP-030-DC24) thermal mass flowmeters and into the MAX200. The MAX200 system can handle air, nitrogen, and carbon dioxide.

The vacuum chamber is maintained at low pressure with an Edwards E2M275 rotary vacuum pump. The exhaust from this pump is ducted to the room's gas removal system. Initial testing of the vacuum system showed that in its as-built configuration, the chamber pressure remains below approximately 3 kPa throughout the duration of the test. Additional testing is ongoing and potential modifications to increase the conductance of the system are being considered.

C. Motion Control System

Work has continued on motion control since the overall description of the upgrade given in Ref. 2. The mARC II motion control system (Fig. 4) consists of two pneumatic cylinders with attached stings for model dwells within the jet and one servo motor controlled sweep arm that rotates a sensor through the jet. Control of the cylinders is achieved with servo valves, and the servo motor is controlled by a programmable servo controller (Parker Aries). The system also controls a gate valve between the vacuum pump and the chamber and a vent valve between the chamber and the exhaust system.

The sensor sweep system is fully designed and has undergone benchtop testing. It is scheduled for installation and initial testing in the near future. Control of the pneumatic cylinders is fully designed and the cylinders are installed on the chamber. Operation of these cylinders, however, is awaiting the design and fabrication of model stings.

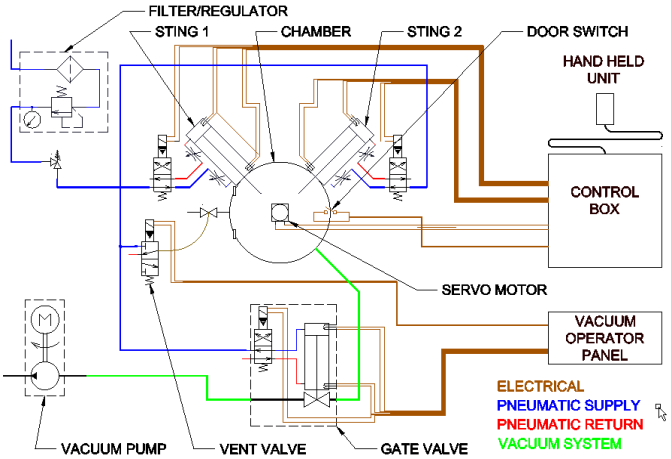

Figure 4: mARC II Control System

The control system is comprised of two parts. The Control Box manages the stings, which insert models into the plasma stream for a specified duration. It also operates the servo controller, which sweeps a sensor through the stream

at certain angular velocities. Simultaneously, the Control Box sends signals to the data acquisition system to initiate the logging of data. The Vacuum Operator Panel runs the gate and vent valve that control the pressure level in the chamber.

All of the functions related to model or sensor insertions can be controlled by the programmable servo controller. This controller has input and output bits that are used to actuate the stings as well as control the sweep with several sweep speeds. Additionally, there are built in timing cycles that eliminate the need for tuning timing circuits. This arrangement is quite flexible since the programming can be revised to accommodate future requirements. A hand held unit is also included for manually positioning the models prior to a run.

A number of safety features are incorporated into the system. A sensor on the door of the chamber prevents the stings and sweep from functioning when the door is open. For the purpose of positioning models this can be overridden by a keyed switch on the hand held unit. Additionally, the software is written such that the next action can only be taken after a sting is fully retracted or a sweep completed.

In its current configuration the program consists of three parts (Fig. 5). The program's first task is to move the sweep arm to a predetermined position referred to as zero degrees. The program then gives the user a choice between sting or sweep operation. Upon choosing sting, the user selects which sting and manual or timed operation. If manual is chosen, the sting is inserted when a keyboard key is pressed and retracted when the key is pressed again. If timed operation is chosen, the user is prompted for an insertion time which is implemented when a key is pressed. If the user selects sweep, the program asks for the selection of one of three sweep speeds (30, 45, and 60 in/sec). Once the sweep speed is selected, then pressing a key implements the sweep. When the sting arm is fully retracted or the sweep is completed, the program prompts the user to either continue or exit. Selecting continue sends the program back to the selection of sting or sweep. As the program executes, it sends output bits to the data logging system indicating whether a sting or sweep operation is occurring. It also produces a signal to indicate the duration during which data should be gathered.

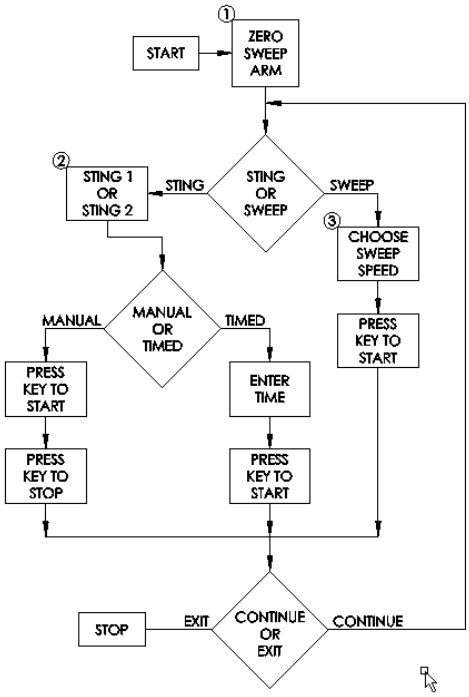

Figure 5: Program Flow Chart

C. Data Acquisition

The mARC II data acquisition consists of a National Instruments (NI) USB cDAQ-9174 chassis inherited from the first-generation mARC system. The cDAQ-9174 contains four sub-modules: NI-9215, NI-9215, NI-9205, and NI-

9205. Together, these offer 8 differential channels (±10 V, 16 Bit, 100 kS/s/ch, screw terminals), 32 single-ended channels (±200 mV; ±1 V; ±5 V; ±10 V, 16 Bit, 250 kS/s/ch, spring terminals), and 16 thermocouple channels with three internal cold-junction compensation channels (±78 mV, 24 Bit, 100 S/s, screw terminals).

The system signal to noise ratio has been improved over the first-generation system by approximately a factor of three through the systematic removal of ground loops, the use of coaxial cable, and improved shielding around sensitive equipment. Due to these improvements, the startup transients from the power supply that caused damage to a previous data system have been mitigated and the manual patch panel which was previously used to isolate the data acquisition system during startup has been removed. This allows continuous data acquisition throughout startup.

Data are acquired at 500 Hz for a number of standard system parameters, including arc current, arc voltage, supply gas mass flowrates, column pressure, chamber pressure, the temperature difference between arc column inlet and outlet cooling water, and temperatures of the chamber and vacuum pump. The temperature difference across the cathode coolant inlet and outlet is recorded at 1 Hz on a battery-powered data logger (Omega RDXL6SD-USB) for isolation since the thermocouples used for these measurements are embedded in the MAX200 power supply system. Additional flow diagnostics can be added to this set as requested or provided by the principle investigator.

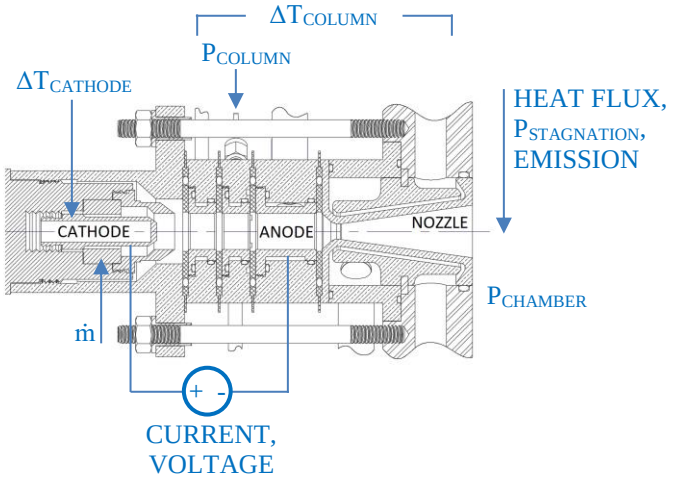

Figure 6: Schematic of Measurements Taken during mARC II Operation

Table 1: List of Measurements Taken during mARC II Operation

Measurement	Description	Units	Instrument
U	Arc voltage	V	Ohio Semitronics VT7-007E-11-TP
I	Arc current	A	Ohio Semitronics CTL-401S/300 and CTA 201H
$\dot{m}_{gas}$	Test gas mass flow rate	g/s	Sage SIP-030-DC24-AIR
P_{column}	Column pressure	Pa	Setra Model 730 SN 6976651
$P_{chamber}$	Vacuum chamber pressure	Pa	Inficon CDG025D, 0-10 Torr + 0-1000 Torr
$P_{stagnation}$	Stagnation pressure	Pa	to be included in once sweep is operational
q	Heat flux in plasma jet	W/cm^2	to be included in once sweep is operational
$\Delta T_{cathode}$	Temperature difference between the cathode coolant supply and return	K	Type K thermocouples and Omega RDXL6SD-USB temperature logger
ΔT_{column}	Temperature difference between the water supply and return manifolds for arc heater cooling	K	E&C Company Thermoducer 8 SN H7
$\dot{V}_{column}$	Volume flow rate of cooling water through the column, anode, and nozzle	l/m	Omega FTB795
VIS	Visible emission	mW/cm^2 µm sr	Ocean Optics STS-VIS

Note: The designation "column" for temperature difference and mass flow rate refers to the cooling loop that actually cools the column, the anode, and the nozzle.

III. Performance Characterization

A. Arc Jet Performance Characteristics

Arc jet performance characteristics are calculated from the measured quantities listed in Table 1. The bulk enthalpy of the flow can be determined by a variety of methods. Presented here are two of the more commonly used methods.

1. Sonic Flow Method [4]

$$h_{sonic\ flow} = \left(280 \frac{A^* p_{column}}{\dot{m}_{gas}}\right)^{2.52} \quad \text{Eq. 1}$$

2. Enthalpy by Energy Balance (EB2) [5]

$$h_{EB2} = \frac{P_{total} - P_{lost\ to\ cooling}}{\dot{m}_{gas}} \quad \text{Eq. 2}$$

Power is delivered to the flow through the arc, so total power is simply the product of current and voltage. In mARC II, power losses from the flow occur from two cooling loops. One loop cools only the cathode while the other cools the rest of the arc heater, the anode, and the nozzle. Energy lost to each of the loops can be calculated using Eq. 3.

$$P_{cooling} = \dot{m}_{cooling} c_p \Delta T \quad \text{Eq. 3}$$

A third method of determining enthalpy utilizing heat flux and stagnation pressure sweeps will be added for future tests (ASTM E637-05, Ref. 6).

Arc jet thermal efficiency is the ratio of power that ends up in the flow to the total power of the arc. It is calculated from Eq. 4.

$$\eta_{AJ} = \frac{\dot{m}_{test\ gas} h}{P_{total}} \quad \text{Eq. 4}$$

B. Horn/Hartman Correlations

In the early 2000's, Horn and Hartman [7] compiled a subset of measured data from four arc jets (AHF, IHF, Scirroco, and a 1-in Sandia heater) and produced correlations that predict expected values for four dependent variables (enthalpy, arc voltage, column pressure, and arc jet efficiency) based on known values for five independent variables (test gas mass flow rate, arc current, constrictor diameter, nozzle throat diameter, and arc length). The resulting correlations (Eq. 5-8) have been employed here to confirm that the mARC II is performing as expected for its geometry. The units in Eqs. 5-8 are listed here just as they were given in Ref. 7.

$$P(atm) = 3.5492 * \dot{m}(lbm/sec)^{0.9825} * I(A)^{0.2481} * D_{con}(in)^{0.4358} * L(in)^{-0.0543} * D^*(in)^{-2.4129} \quad \text{Eq. 5}$$

$$V(kV) = 2.0419 * \dot{m}(lbm/sec)^{0.6649} * I(A)^{-0.0829} * D_{con}(in)^{0.8559} * L(in)^{0.3273} * D^*(in)^{-1.2408} \quad \text{Eq. 6}$$

$$H(BTU/lbm) = 36.765 * \dot{m}(lbm/sec)^{-0.1008} * I(A)^{0.5769} * D_{con}(in)^{-0.7669} * L(in)^{0.3575} * D^*(in)^{-0.3159} \quad \text{Eq. 7}$$

$$\eta = 17.023 * \dot{m}(lbm/sec)^{0.2330} * I(A)^{-0.3303} * D_{con}(in)^{-1.6364} * L(in)^{0.0366} * D^*(in)^{0.9193} \quad \text{Eq. 8}$$

IV. Results

Test conditions for an arc jet are set by specifying the desired arc current and test gas mass flow rate. To explore the test envelope of the mARC II system, initial testing was carried out over the entire range of arc currents sustainable by the MAX200 power supply (40, 100, 160, and 200A) and a wide range of test gas mass flow rates (0.25, 0.5, and 0.8 g/s). The test gas for all of these initial tests was air. Test duration for all tests was 60 sec, which began after the startup process and once steady-state conditions were reached.

Sample data traces for one run (100 A and 0.25 g/s air) are shown in Fig. 7. The steady state test time begins when the mass flow rate settles such that its derivative does not surpass ± 3e-4 g/s^2. The mean values used to calculate performance parameters (from Eqs. 1-4) are extracted from measured data such as those shown in Fig. 7, with the exception of the cathode cooling loop flow rate, which is provided in the Hypertherm MAX200 manual and remains constant at 3 L/min. Mean and standard deviation values for each measured quantity are calculated over the 60 sec steady-state time shown. Most measured quantities remain relatively constant throughout the steady-state period. However, the chamber pressure measurements continually increase over the test time, as does the temperature difference across the cathode, which has a very slow response time. The pressure rise throughout the test is attributed to the low conductance of the vacuum system and will be discussed later. The cathode temperatures respond slowly because they are measured at the MAX200 and it takes a significant portion of the run for the long cooling lines to reach equilibrium such that they no longer impact the measured temperature difference. The mean cathode temperature difference is therefore calculated over only the last 10 seconds of test time.

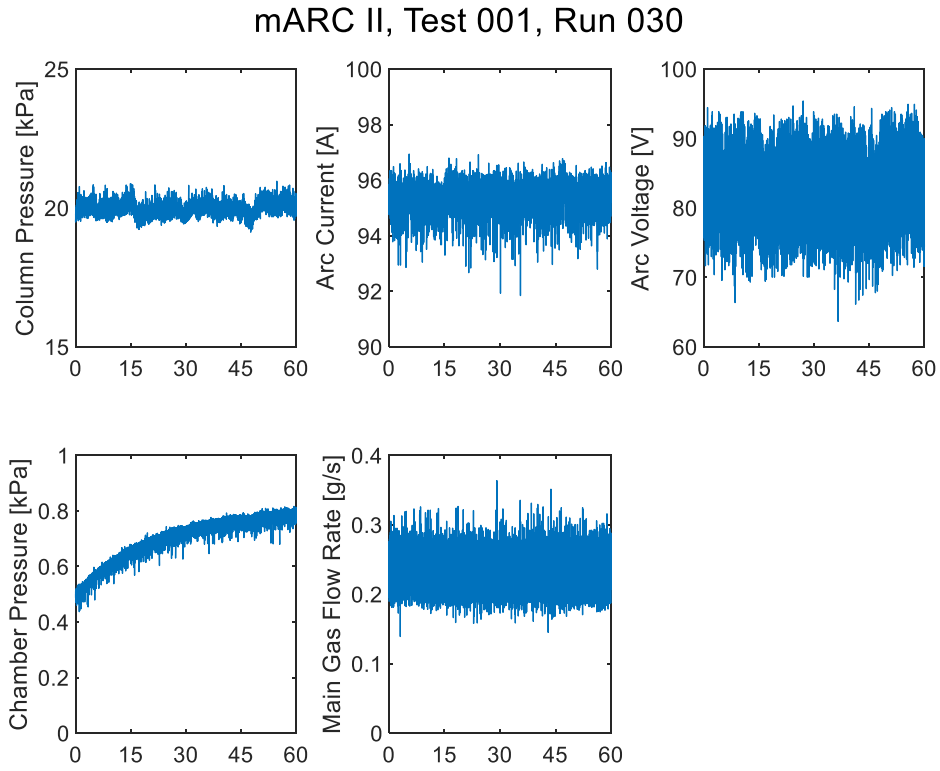

Figure 7: Sample data traces for a mARC II run (100 A, 0.25 g/s air).

Figure 7 shows only the steady-state test time. Initial mass flow rate transients during startup are shown in Fig. 8 for three runs carried out at a set current of 100 A. The MAX200 system tends to initially overshoot the desired set point before achieving its steady state test condition within 20-30 sec. This startup phase can be seen in the Fig. 8 traces.

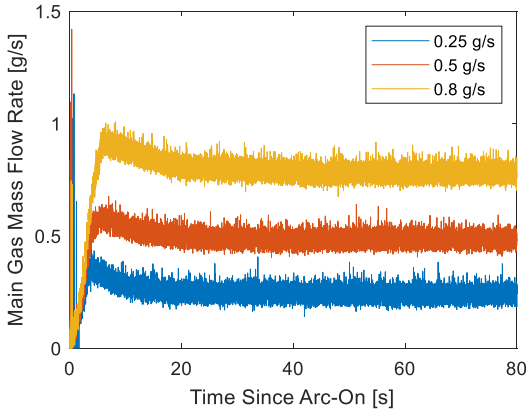

Figure 8: Measured air mass flow rate, 100 A (Runs 22, 23, 24)

The measured chamber pressure for those same three 100 A runs is shown in Fig. 9. As expected, when the flow rate of gas into the chamber is increased, the plateau value of chamber pressure also increases. However, Fig. 9 shows clearly that the chamber pressure rises continuously during the duration of these runs. Ideally, the vacuum system would maintain a relatively steady pressure throughout the test. The team is currently working to modify the system such that conductance can be increased and a lower chamber pressure can be maintained throughout the test duration.

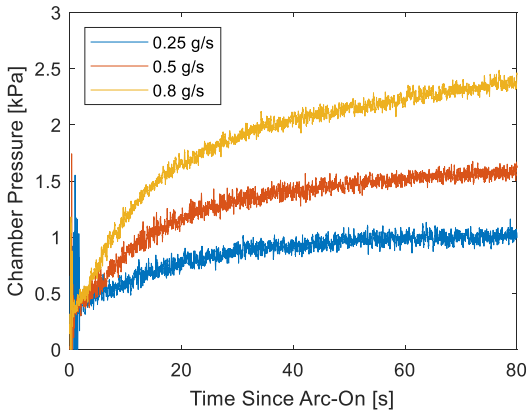

Figure 9: Measured chamber pressure rise at current setting = 100 A

The measured arc current for this first set of mARC II runs is shown in Fig. 10. This figure includes data taken at all three of the mass flow rate settings. For the 40 A set point, the measured current falls slightly above the set current, but as current increases, the measured values fall well below the set point. This could be an inherent behavior of the MAX200 power supply, or it could be within the measurement uncertainty of the current sensor. Data from the first-generation mARC (Ref. 3) show only a small deviation from set point. The measured current was approximately 2 A higher than the set point for all reported currents. However, the first-generation mARC data only go as high as 100 A, and the deviation from set point seems to get more significant above this current. Of the 13 total runs shown here, six of them were at 100 A, and that setting shows the most scatter. As additional testing is carried out at mARC II, especially at higher currents, the source of this difference will undoubtedly become clearer.

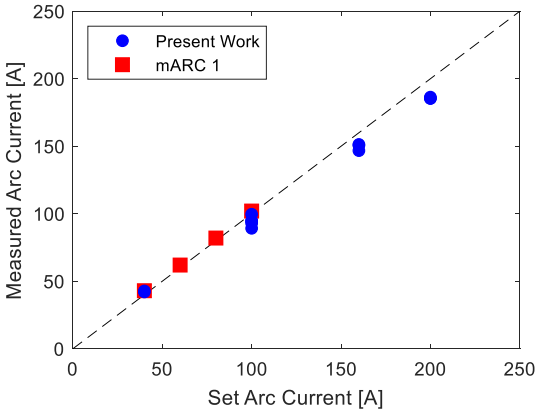

Figure 10: Deviation from current set point, data from the first generation mARC taken from Ref. 3

One possible explanation for deviation from set point comes when studying how the measured current changes with accumulated time on the cathode. Although the anode has been designed for extended use, the cathode is a consumable part of the Hypertherm system that is designed to be replaced relatively frequently. Nawaz et al. [3] indicate that the cathode should be replaced after approximately 90 minutes of accumulated run time. The cathode used for these initial runs has only accumulated approximately 20 minutes of run time, but even within that period some trends have become apparent. Figure 11 shows 13 runs across all four current settings. Some of the runs were performed within the same day, but in that case the arc was extinguished between each run allowing the chamber pressure to drop to below 13 Pa before beginning the next run. Additional data will help clarify this trend, but the 40 A, 100 A, and 160 A settings all seem to show a slight decrease in measured current as accumulated cathode time increases. The measured current at the 200 A setting remains relatively constant. Figure 11b shows how the difference between the set current and measured current varies as total cathode time accumulates. Over the first 600 sec of run time, the measured current drops continuously. However, after the 600 sec point the difference between the set and measured currents begins to level out.

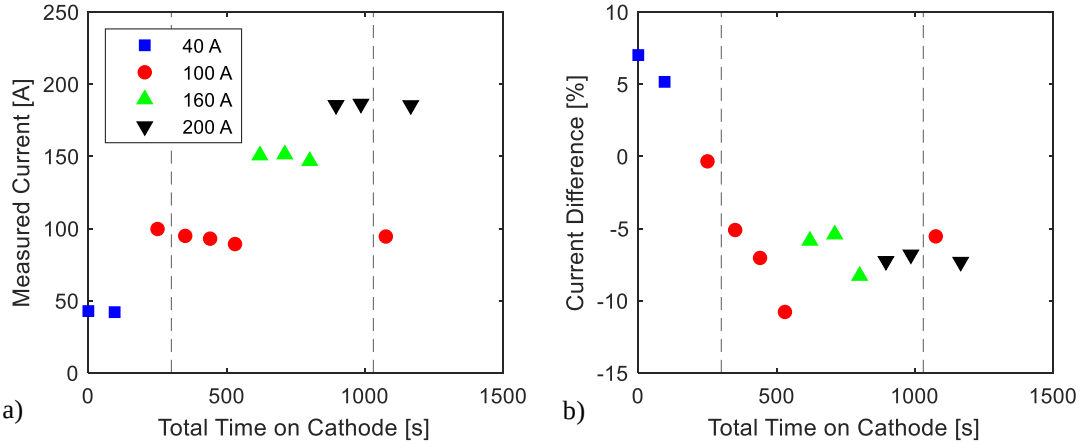

Figure 11: Accumulated run time on cathode, a) measured current, b) difference between set current and measured current. Data were taken over three different days. Dashed vertical lines delineate the different days.

The measured arc voltage for all runs is shown in Fig. 12. In Fig. 12a, for a given mass flow rate, arc voltage decreases slightly as current is increased. This was also observed and reported in Ref. 3. This is expected given the mARC heater geometry. In the mARC II heater, the downstream end of the arc is free to attach at any point within the length of the anode, and the anode length is over half of the total column length (see Fig. 2). As current is increased, the temperature within the column increases and plasma resistivity decreases. This leads to a drop in arc voltage and, since the arc length is free to vary significantly, a decrease in the arc length. It should be noted that for large arc heaters (with meters long constrictors) the voltage drop with increasing current is minimal since the electrode length is such a small fraction of the total arc length.

Figure 12b shows that for a given current setting, the voltage required to maintain the arc increases with increasing air mass flow rate. This figure illustrates why the power supply is unable to maintain an arc at 0.8 g/s and 40 A. The voltage required at those conditions would be over its 150 V maximum.

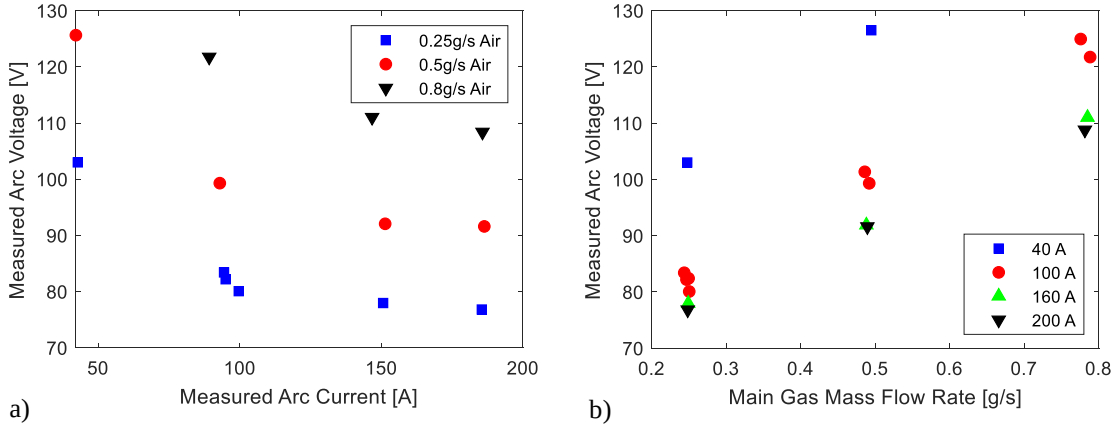

Figure 12: Dependence of arc voltage on a) arc current, b) mass flow rate

Column pressure also depends on both the current and the test gas mass flow rate. For a given mass flow rate, as arc current is increased, column pressure increases approximately linearly (Fig. 13a). For a given current setting, as mass flow rate is increased, column pressure also increases linearly (Fig. 13b).

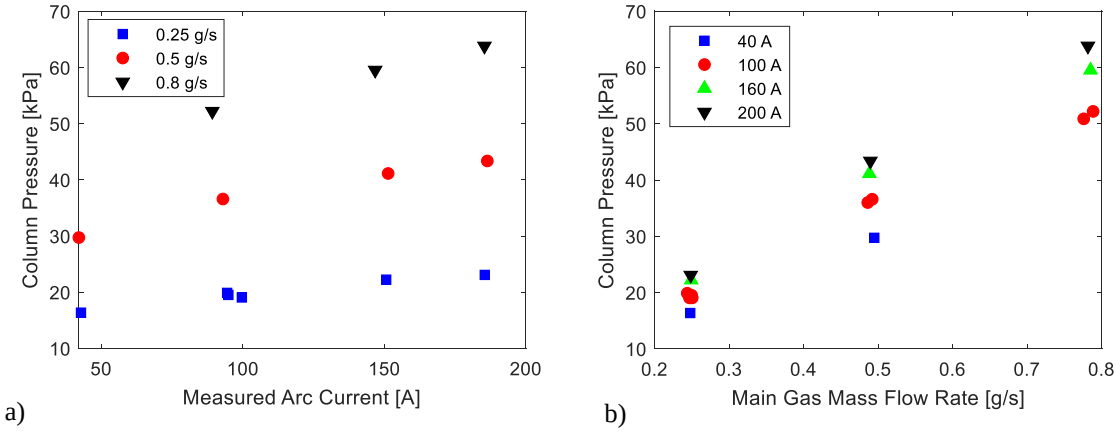

Figure 13: Dependence of column pressure on a) arc current, b) mass flow rate

Arc jet performance parameters are calculated for these runs. Enthalpy comparisons with the published data from the first-generation mARC [3] show that for mARC II, the range of accessible bulk enthalpies for a given power setting (Fig.14a) has shifted down. This is due to the additional water cooling in the mARC II heater and nozzle, and provides desired access to lower-enthalpy flows. The higher-enthalpy region can still be accessed by adding a third constrictor disk and increasing the total power delivered to the flow. The two-disk configuration can only reach approximately 20 kW out of the 30 kW provided by the power supply. The added water-cooling of mARC II should allow reasonable run times for these high-power runs. The three-disk configuration is planned for future work.

Figure 14b shows how enthalpy depends on column pressure for all three mass flow rates studied here. Data from the first-generation mARC were taken at three mass flow rates, as well, but only one of these (0.25 g/s) matches a rate studied in the present work. Data from Ref. 3 for that matching mass flow rate is included in Fig. 14b. The comparable data from the two different mARC configurations clearly fall along the same trend line, with the notable difference that mARC II can reach lower enthalpy values and lower column pressures. As discussed above, for a given arc jet

power, slightly more energy is removed from the gas flow with the added water cooling of mARC II, thus the lower enthalpy. This also means that the gas does not expand quite as much within the column, corresponding to a lower column pressure.

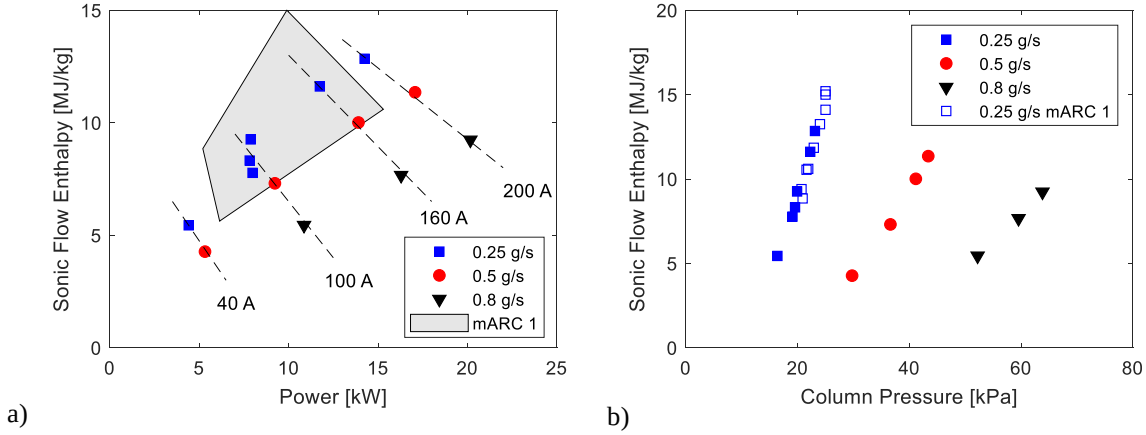

Figure 14: mARC II enthalpy envelope, data from the first generation mARC taken from Ref. 3

The mARC II efficiency lies between 0.2 and 0.4 (Fig. 15). Reference 7 reports that constricted arc heater efficiencies generally lie in the 0.25 to 0.6 range. The mARC II heater is on the lower end of that range, but still well within reasonable bounds. The first-generation mARC efficiency is also plotted in Fig. 15. It lies just above the mARC II level. More components of mARC II are water-cooled than the previous system, therefore the resulting flow enthalpy is slightly lower than the first-generation mARC. This results in a slightly lower arc jet efficiency, but was nonetheless judged to be worthwhile in order to both increase the run time capability of mARC II, access lower bulk enthalpies, and obtain a more accurate value of bulk enthalpy from the EB2 method.

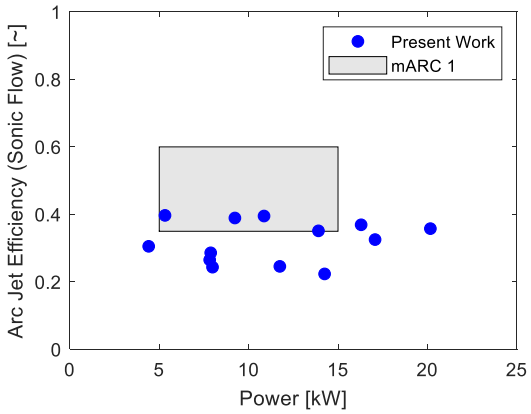

Figure 15: mARC II efficiency, data from the first generation mARC taken from Ref. 3

Data from the present work has been run through the Horn/Hartman correlations to see how mARC II performance compares to the four arc jets used to compile the correlations. A subset of the data that went into the correlations is included in Fig. 16, as well, for reference. Including all of the arc jet data provided in Ref. 7 would crowd these correlation figures, so only the AHF data is included here. The necessary unit conversions have been carried out to produce Fig. 16 in SI units.

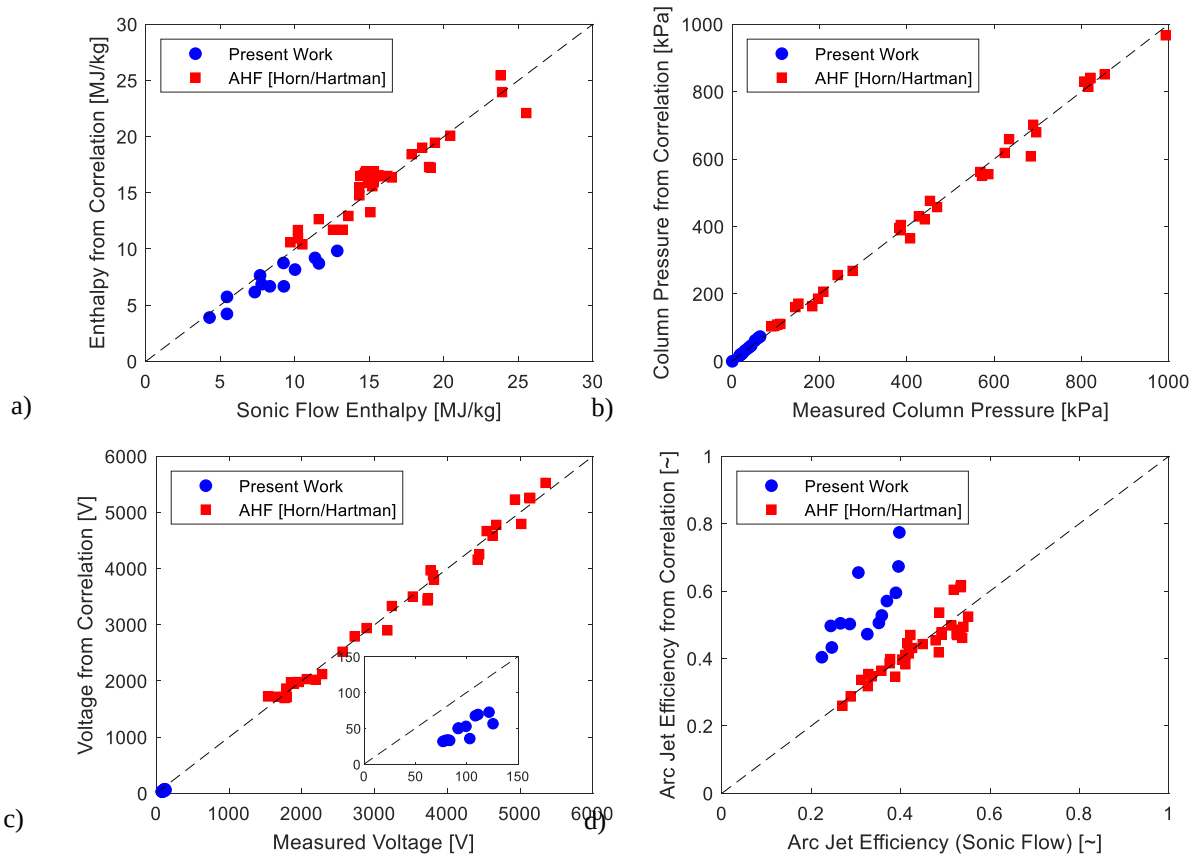

Figure 16: Horn/Hartman correlations for data from present work

The sonic flow enthalpy and measured column pressure in the present work are described well by the Horn/Hartman correlations. The enthalpy correlation predicts the sonic flow enthalpy to within 14% and the column pressure correlation predicts the measured column pressure to within 7%. However, the voltage correlation underpredicts the mARC II measured voltage by approximately 50%. The cause of this difference was discussed earlier. Since the mARC II has a relatively long anode compared to its total constrictor length, its voltage behavior is different than the behavior of the larger arc jets that were used to compile these correlations. This same reasoning also explains the efficiency plot. Since the correlation underpredicts the measured voltage and voltage is in the denominator of the efficiency equation, it stands to reason that the correlation would overpredict the arc jet efficiency. Nonetheless, comparisons with these correlations instill confidence that the mARC II is producing reasonable results. Enthalpy and column pressures match well with expected values. The geometric differences between the arc heaters used to compile the correlations and the mARC II readily explain the discrepancies between the correlations and the mARC II measured voltage and inferred efficiency.

These initial runs included a visible spectrometer, and a separate publication covering these initial mARC II optical emission spectroscopy measurements is currently in the review process [8]. Spectra were measured through one of the four windows that provide optical access to the jet as it exits the nozzle. Examples of the spectra reported in Ref. 8 are shown in Fig. 17. For all of these runs, elements such as copper, silver, sodium, lithium and potassium are observed in the flow. For combinations of high current and/or high mass flow rate, the atomic oxygen line appears initially quite strongly, and its intensity decreases throughout the duration of the run (Fig. 17a). Copper and silver are constituents of the electrodes, and they can be seen in the visible spectra (Fig. 17b). Sodium, lithium, and potassium are strong emitters in the visible, and their measurement here may be due to very small amounts present in the air near sea-level.

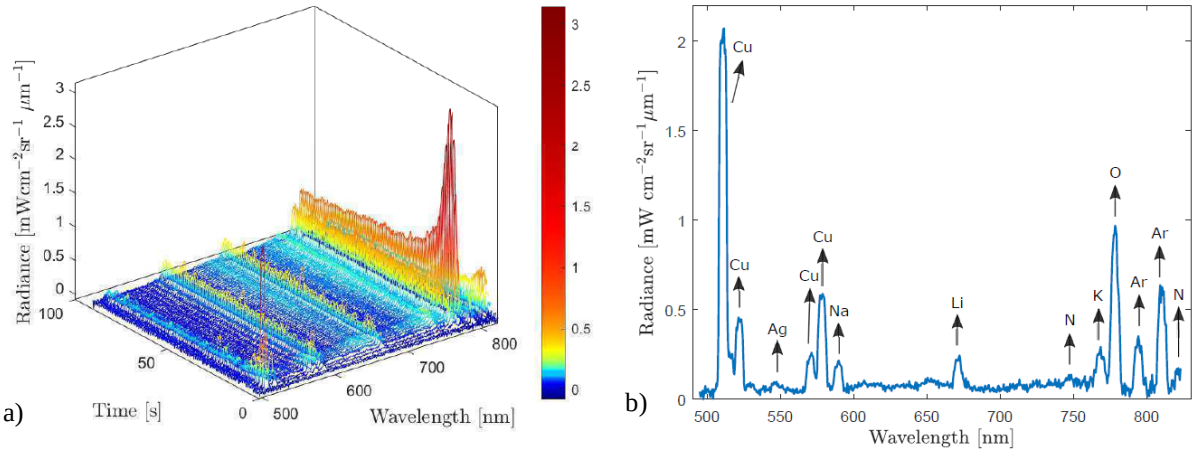

Figure 17: Optical emission spectroscopy measurements in the visible region (100 A, 0.5 g/s air), a) entire test time, b) time instant t = 4.1 s. (Ref. 8)

V. Simulation

The flow through the nozzle and into the chamber is simulated using the Data Parallel Line Relaxation (DPLR) code. Solutions clearly show overexpanded flow due to the higher-than-anticipated chamber pressure. As mentioned above, the team is working to ensure that this chamber pressure is lowered for future testing.

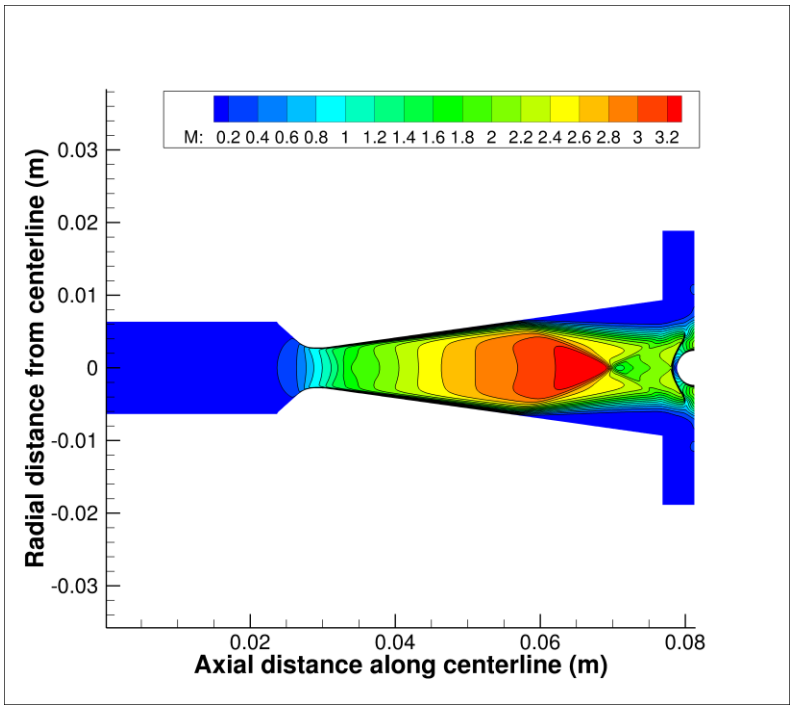

Figure 18: Steady-state flow field for 40 A, 0.25 g/s air, 16.4 kPa column pressure, 0.75 kPa chamber pressure

VI. Conclusion

Construction is complete at the mARC II facility. Integrated systems testing is complete with the exception of the model insertion system. Work to bring this system online is ongoing.

Initial characterization of the facility with air is presented along with comparisons to the first-generation mARC and to larger arc jet facilities. Initial facility health data show expected trends in the relationships between current, test gas mass flow rate, column pressure, enthalpy, and arc power. The enthalpy range in the present two-disk configuration is approximately 4 – 13 MJ/kg, slightly lower than the first-generation mARC because more components of the heater are cooled in mARC II. The two-disk configuration only uses approximately 20 kW out of the 30 kW available from this power supply, so it is feasible to push that upper limit to enthalpies above 13 MJ/kg with the addition of a third constrictor disk. Comparisons with correlations that were developed to describe larger arc jets show excellent agreement for enthalpy and column pressure, while the difference between voltage data from the present work and the correlation is easily explained by a difference in geometry between this miniature arc jet and the much larger facilities used to derive the correlation.

The team is currently working to complete the last few tasks related to integrated systems testing. Chamber pressure during runs is higher than optimal, leading to an overexpanded jet for all conditions studied. The team is working on methods to lower the chamber pressure for future runs. Once this occurs and mARC II is fully characterized, it will be added to the available entry testing facilities operated by the Thermophysics Facilities Branch.

Acknowledgments

M.E. MacDonald, D.E. Schickele, and J. Hartman are supported through the NASA NNA16BD26C contract. M.A. Haw is supported through the NASA NNA15BB15C contract. D. Luis is the recipient of a research fellowship (SFRH/BI/150289/2019), funded by Fundação para a Ciência e Tecnologia (FCT, Portugal). The authors would like to thank the Entry Systems Division and Thermophysics Facilities Branch for their support throughout this upgrade. In particular, the authors would like to thank Thanh Ho, Ramon Martinez, Rick Ryzinga, Brandon Ross, Austin Ng, Matthew Hoffer, Nicholas Reed, James Hope, Austin Proft, Justin Franklin, Sami Karam, Josh Kaufmann, Haneo Shim, John Anacleto, Eric Noyes, Trent Hughes, Michael Claassen, Cesar Acosta, and Patrick Viruel for their work to disassemble the previous system and bring the new system online.

References

[1]Terrazas-Salinas, I., "Test Planning Guide for NASA Ames Research Center Arc Jet Complex and Range Complex," A029-9701-XM3 Rev. F, <https://www.nasa.gov/sites/default/files/atoms/files/tsf_test_planning_guide_revf.pdf>, accessed March 2020.

[2]MacDonald, M.E., Philippidis, D., Ho, T.S., Haw, M., Hartman, J., McGlaughlin, M.S., "Build-up of the second-generation 30 kW miniature arc jet (mARC II) at NASA Ames Research Center," AIAA 2019-2857, AIAA Aviation Forum, Dallas, TX, 2019.

[3]Nawaz, A., Ho, T.S., Philippidis, D., Hartman, J., McGlaughlin, M.S., Driver, D.M., "Baseline characterization of the 30kW miniature arc jet facility mARC at NASA Ames," AIAA 2016-3819, 32st AIAA Aerodynamic Measurement Technology and Ground Testing Conference, Washington, D.C., 2016.

[4]Winovich, W., "On the equilibrium sonic-flow method for evaluating electric-arc air-heater performance," NASA TN D-2132, 1964.

[5]"Standard Practice for Measuring Plasma Arc Gas Enthalpy by Energy Balance", ASTM Standard Designation: E 341-96, American Society for Testing and Materials, West Conshohocken, PA, 1996

[6]ASTM E637-05(2011), Standard Test Method for Calculation of Stagnation Enthalpy from Heat Transfer Theory and Experimental Measurements of Stagnation-Point Heat Transfer and Pressure, ASTM International, West Conshohocken, PA, 2011,

[7]Horn, D., Hartman, J., "Arcjet Performance and Design Considerations," private communication, March 2020.

[8]Luis, D.Z.F., MacDonald, M.E., "Emission Spectroscopy Characterization of Electrode Species in the Freestream Flow at the NASA Ames Miniature Arc Jet II Facility," for submission to Journal of Quantitative Spectroscopy and Radiative Transfer, 2020.

[9]Wright, M.J., White, T., Mangini, N., "Data Parallel Line Relaxation (DPLR) Code User Manual: Acadia – Version 4.01.1," NASA Technical Memorandum TM-2009-215388, 2009.

[10]Wright, M.J., Candler, G.V., Bose, D., "Data-Parallel Line Relaxation Method for the Navier-Stokes Equations," *AIAA J.*, Vol. 36, No. 9, pp. 1603-1609, 1998.